Geophysical Research Letters

RESEARCH LETTER
10.1029/2021GL093879

Duration of Individual Relativistic Electron Microbursts: A Probe Into Their Scattering Mechanism

M. Shumko[1,2], L. W. Blum[3], and A. B. Crew[4]

[1]NASA's Goddard Space Flight Center, Greenbelt, MD, USA, [2]Universities Space Research Association, Columbia, MD, USA, [3]University of Colorado Boulder, Boulder, CO, USA, [4]Johns Hopkins University Applied Physics Laboratory, Laurel, MD, USA

Key Points:

- We identified relativistic microbursts observed by the Solar Anomalous and Magnetospheric Particle Explorer satellite and quantified their duration
- The microburst duration interquartile range is 70–140 ms and shows trends in Auroral Electrojet, L-shell, and magnetic local time (MLT)
- In MLT, microburst durations double between midnight and noon-a trend similar to chorus element durations

Correspondence to:
M. Shumko,
msshumko@gmail.com

Citation:
Shumko, M., Blum, L. W., & Crew, A. B. (2021). Duration of individual relativistic electron microbursts: A probe into their scattering mechanism. *Geophysical Research Letters*, *48*, e2021GL093879. https://doi.org/10.1029/2021GL093879

Received 14 APR 2021
Accepted 17 AUG 2021

Abstract We used the Solar Anomalous and Magnetospheric Particle Explorer to identify and quantify the duration of relativistic, >1 MeV, electron microbursts. A typical relativistic microburst has a ≈100 millisecond (ms) duration, and the interquartile range of the duration distribution is 70–140 ms. We investigated trends in the microburst duration as a function of geomagnetic activity, L-shell, and magnetic local time (MLT). The clearest trend is in MLT: the median microburst duration doubles from 75 milliseconds at midnight to 140 milliseconds noon MLT. This trend is similar to the whistler mode chorus rising tone element duration trend, suggesting a possible relationship.

Plain Language Summary Energetic electron microbursts are an intense form of naturally occurring particle precipitation from the outer Van Allen Radiation Belt into Earth's atmosphere. Microbursts are observed in, or just above, the Earth's atmosphere, and are characterized by their short duration in time series data, often defined to be less than a second. The impact of microburst precipitation on the Earth's atmosphere is uncertain, but has been predicted to substantially degrade mesospheric ozone through the production of odd nitrogen and odd hydrogen molecules. Besides their environmental impact, we don't comprehensively understand how plasma waves, such as whistler mode chorus waves, scatter microbursts into our atmosphere. Therefore, in this study we quantified the duration of microbursts and used it as a proxy to understand how microbursts are scattered by these waves. We found that the microburst and chorus wave durations are correlated: their duration roughly doubles between the anti-sunward and sunward regions of the outer radiation belt.

1. Introduction

Earth's outer Van Allen radiation belt electron population is in constant flux, controlled by processes such as, radial transport, injections from the magnetotail, magnetopause shadowing, as well as local heating and loss into Earth's atmosphere due to wave-particle interactions (e.g., Ripoll et al., 2020, and references within). Whistler mode chorus is one type of plasma wave, characterized by subsecond rising tone elements, that plays a dual role in electron dynamics: accelerate electrons from 10s of keV to MeV energies, and pitch angle scatter electrons into the atmosphere (e.g., Horne & Thorne, 2003; Li et al., 2009; Summers, 2005; Thorne, 2010). One form of electron precipitation believed to be generated by chorus are microbursts: a subsecond intense increase of electrons. Microbursts were first observed by balloons in Earth's upper atmosphere, and later by satellites in low Earth orbit (LEO) (e.g., Anderson & Milton, 1964; Blake et al., 1996; Douma et al., 2017; Kurita et al., 2016; Lorentzen et al., 2001; O'Brien et al., 2003; Winckler et al., 1962), and recently at high altitude near the magnetic equator (Shumko et al., 2018).

Microburst electron energies span multiple orders of magnitude from tens of keV observed by, for example, Datta et al. (1997), to >1 MeV observed by the Solar Anomalous Magnetospheric Particle Explorer (SAMPEX) by Blake et al. (1996). Microbursts are predominately observed outside the plasmapause on the outer radiation belt footprints, $L \approx 4-8$, and in the midnight to morning Magnetic Local Times (MLT) (≈0 – 12 hours MLT) (Blum et al., 2015; Douma et al., 2017; Lorentzen et al., 2001; O'Brien et al., 2003). While microbursts are observed under all geomagnetic conditions, Douma et al. (2017) showed that microburst occurrence frequency dramatically increases with the Auroral Electrojet (AE) index, and O'Brien et al. (2003) showed a similar trend with the microburst frequency with the Disturbance storm time index phase.

The relative impact of energetic electron precipitation on the ionization of Earth's atmosphere and the depletion of radiation belt electrons is uncertain, but is estimated to be substantial. Duderstadt et al. (2021) showed observations that suggest that electron precipitation can significantly impact atmospheric composition. The authors estimated a 20%–30% increase in atmospheric odd nitrogen (NO_X), causing a 1% decrease in ozone (O_3)—substantial enough to affect the radiative balance in the upper atmosphere. Microbursts have also been estimated to be able to deplete the outer radiation belt electrons in hours to a few days, and models predict depletions of up to 20% of upper mesospheric O_3 (Breneman et al., 2017; Douma et al., 2019; O'Brien et al., 2004; Seppälä et al., 2018; Thorne et al., 2005).

Electron microbursts are widely believed to be scattered by chorus waves. They were associated early on, due to the similar duration of microbursts and chorus rising tone elements and a similar occurrence distributions in MLT and L-shell (e.g., Lorentzen et al., 2001). Furthermore, Breneman et al. (2017) associated chorus rising tone elements to microbursts observed by the Focused Investigation of Relativistic Electron Bursts: Intensity, Range, and Dynamics CubeSats (FIREBIRD-II; Crew et al., 2016; Johnson et al., 2020) during a close magnetic conjunction.

A natural follow-on question is how are microbursts generated by chorus rising tone elements? For example, it is still unclear if relativistic (>1 MeV) microbursts are scattered via cyclotron resonance at high magnetic latitudes, or a higher resonance harmonic near the magnetic equator (Lorentzen et al., 2001). One way to address this question is to study for how long microburst electrons are in resonance with a chorus wave. The resulting microburst duration, that is the microburst width in the time series data, is a probe into the conditions necessary to scatter microburst electrons. Thus, we used SAMPEX data to quantify the distribution of relativistic microburst durations as a function of L-shell, MLT, and the AE index. We then compared these results to prior chorus rising tone element studies, and a chorus-electron test particle model.

2. Instrumentation

For this study, we used the >1 MeV electron data, taken by the Heavy Ion Large Telescope (HILT) instrument (Klecker et al., 1993) onboard the SAMPEX satellite (Baker et al., 1993). SAMPEX was launched in July 1992 and reentered Earth's atmosphere in November 2012. It was in a 520 × 670 km, 82° inclination LEO. In general, SAMPEX had two pointing modes: spin and orbit rate rotation (zenith pointing). To avoid the compounding effects due to the variable pitch angles sampled in the spin mode, we only used the zenith pointing mode data. The International Geomagnetic Reference Field (Thébault et al., 2015) magnetic field model was used to derive the geomagnetic coordinates.

The HILT instrument consisted of a large rectangular chamber with the aperture on one end, and 16 solid state detectors on the other. We used the HILT electron data taken between 1997 and 2012 (state4 in the data archive). The electron counts were accumulated from all of the solid state detectors at a 20 ms cadence.

3. Methodology

3.1. Microburst Identification

First, we identified microbursts using the burst parameter defined by O'Brien et al. (2003), also used in numerous other SAMPEX microburst studies (e.g., Douma et al., 2017). Assuming Poisson probability for the observed electron counts, the burst parameter is the number of standard deviations of a foreground signal above the background, and is expressed as

$$n_\sigma = \frac{N - A}{\sqrt{A + 1}} \tag{1}$$

where N is the number of foreground electron counts, and A is the centered running average background counts. The 1 in the denominator prevents a division by 0 error. In O'Brien et al. (2003), and in the results in this study, N was summed over 100 ms and is called N_{100}, while A was summed over 500 ms and is likewise called A_{500}. Henceforth, we specify the time windows with subscripts for N and A. Times when $n_\sigma > 10$ are classified as burst times, and the peak time in each continuous burst time interval is saved to the microburst

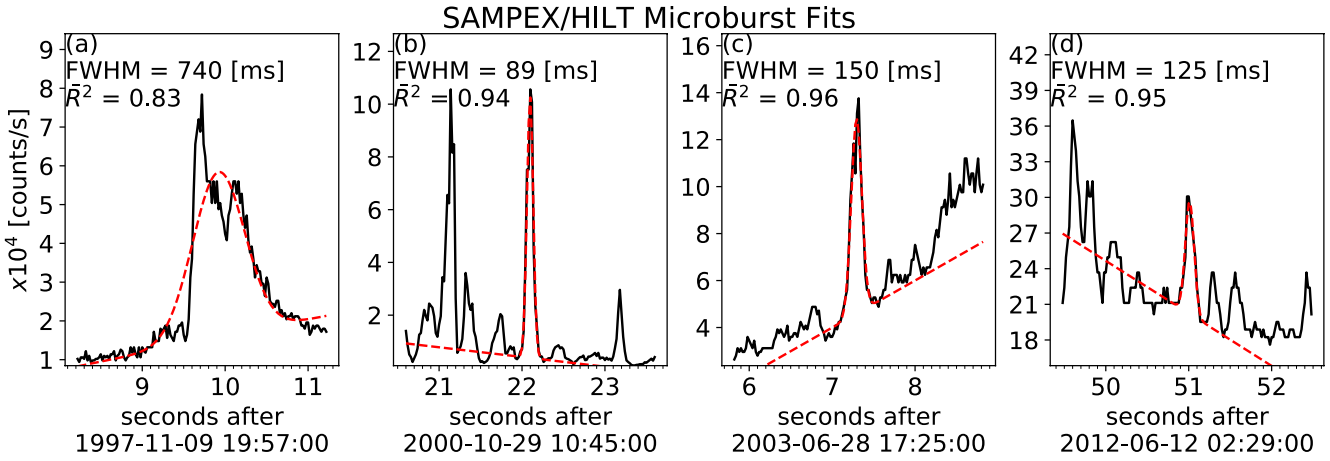

Figure 1. Examples of relativistic microbursts are shown by the black curves, and the fits are shown by the dashed red curves. The fit's full width at half maximum and the $\bar{R}^2$ goodness of fit metric is annotated in each panel. Microbursts with $\bar{R}^2 > 0.9$ were used for this study—hence the two-peaked example in panel a was not analyzed. The major time ticks are at every second, while the minor ticks are at every 100 milliseconds.

data set. With A_{500} and N_{100}, we detected a total of 256,764 microbursts over the 15 year period from 1997 to 2012. Four examples of microbursts are shown in Figure 1 by the solid black curves.

3.2. Microburst Duration Quantification

Second, we estimated the microburst duration using two methods, detailed below, that yielded similar results: the duration at half of the microburst's topographic prominence and the full width at half maximum (FWHM) from a Gaussian fit.

The topographic prominence is a simple and robust method to estimate the microburst duration previously used to identify curtains, a similar-looking type of precipitation (Shumko et al., 2020). Using this technique, we define microburst duration to be the duration at half of the microburst's topographic prominence: the height of the microburst relative to the maximum of the two minima on either side of the microburst peak. On each side of the microburst peak, the minima are searched for between the microburst and a higher peak on that side. While the topographic prominence method of estimating microburst durations is simple and robust, a downside is its inability to automatically verify that the estimated duration is of a single microburst and not a superposition of multiple microbursts (Figure 1a is an example of two superposed microbursts).

To overcome this downside, we fit the microburst time series and used the R^2 goodness of fit metric to verify the fit. We assumed a fit model consisting of a Gaussian to model the microburst peak, superposed with a straight line to model the background counts due to drifting electrons at and around the microburst. This model is defined as

$$c(t|A,t_0,\sigma,c_0,c_1) = Ae^{-\frac{(t-t_0)^2}{2\sigma^2}} + c_0 + c_1 t \tag{2}$$

where A, t_0, and σ are the Gaussian amplitude, center time, and standard deviation; c_0 and c_1 are the linear background count intercept and slope. We determined the number of data points to fit as the maximum of: 4x topographic prominence duration or 500 ms. A challenge to any robust and automated nonlinear regression algorithm is guessing the initial parameters. The initial parameter guesses for the Gaussian are provided by the estimated topographic prominence and duration. The straight line parameter guesses were: c_0 = median(counts) and $c_1 = 0$. The optimal fit parameters were found using scipy's curve_fit() function in Python. We defined the microburst duration as the FWHM of the microburst peak, defined by

$$\text{FWHM} = 2\sqrt{2\ln 2}\sigma. \tag{3}$$

To evaluate the fit, we used the R^2 goodness of fit metric. R^2 is defined as

$$R^2 = 1 - \frac{SS_{res}}{SS_{mean}} = 1 - \frac{\sum(c_i - f_i)^2}{\sum(c_i - \bar{c})^2} \quad (4)$$

where SS_{res} is the sum of the squared residuals between the observed counts c_i and the fit counts f_i for each time step, and likewise SS_{mean} is the sum of the squared residuals between c_i and the mean of the counts, $\bar{c}$.

One interpretation of R^2 is fractionally how much better the variance in the data is explained by the model fit, compared to the null hypothesis horizontal line at $\bar{c}$. R^2 varies from 1 for a fit that perfectly describes the data, to $-\infty$ for poor fits (a fit can be much worse than the mean null hypothesis).

To account for overfitting, we used the adjusted R^2, $\bar{R}^2$, defined as

$$\bar{R}^2 = 1 - (1 - R^2)\frac{n-1}{n-p-1} \quad (5)$$

where n is the number of data points fit, and p is the number of parameters. Intuitively, $n-1$ is the number of degrees of freedom for the null hypothesis, and $n-p-1$ is the degrees of freedom for the fit model. Fits with $\bar{R}^2 > 0.9$ are considered good and are analyzed. As a check, we compared the microburst duration estimated with the prominence and fit methods. We first chose an agreement criterion between the two methods as a duration within 25%; together with the $\bar{R}^2 > 0.9$ constraint, 85% of microbursts satisfied these criteria.

Figure 1a shows an example of two superposed microbursts that had a fit $\bar{R}^2 = 0.83$ that were excluded from this study. On other hand, microbursts in Figures 1b–1d had $\bar{R}^2 > 0.9$ and were included in the following analysis. Lastly, Figures 1c and 1d demonstrate the necessity of the linear fit to account for the changing background. The linear fit accounts for the nonzero mean background counts and the uneven amplitudes at the edges of the Gaussian. Of the 256,764 detected microbursts, 109,231 have $\bar{R}^2 > 0.9$ and are used for the remainder of this study.

4. Results

We used the well-fit microbursts to quantify the distribution of microburst duration (FWHM). We then investigated trends in the duration distribution as a function of the AE index, L-shell and MLT. We begin with the overall microburst distribution.

Figure 2a shows the distribution of all well-fit microbursts. This distribution is strongly peaked with 97 ms median duration. The interquartile range spans about a factor of two in microburst duration, from 66 to 142 ms.

We then investigated the dependence of microburst duration as a function of geomagnetic activity. To be consistent with many prior wave and microburst studies, we use the AE index to quantify the level of geomagnetic disturbance. We adopt the same three AE intensity levels used in prior studies, such as Douma et al. (2017), and Meredith et al. (2020): AE < 100, 100 < AE < 300, and AE > 300, in units of nanotesla (nT). Figure 2b shows the distribution of microburst duration for the three AE categories. The distributions are qualitatively similar, gradually narrowing and shifting to shorter durations with increasing AE. The median microburst duration decreases from 130 ms for AE < 100 to 95 ms for AE > 300.

Next, Figures 3 and 4 show the microburst duration as a function of L and MLT. Figure 3a shows the median microburst distribution, while Figure 4 shows the marginalized distributions as a function of L or MLT. The median microburst duration trend in Figure 3a roughly doubles in MLT: from 75 ms at midnight to 140 ms at noon. In L-shell, the median microburst duration slightly increases with L-shell, most apparent near midnight MLT.

To disentangle the L and MLT distributions, Figure 4 shows the marginalized distributions; MLT was marginalized out (summed over) in Figure 4a and L-shell was marginalized out in Figure 4b. Figure 4a shows a gradual broadening and shifting of the microburst duration in L: the median duration, shown by the solid

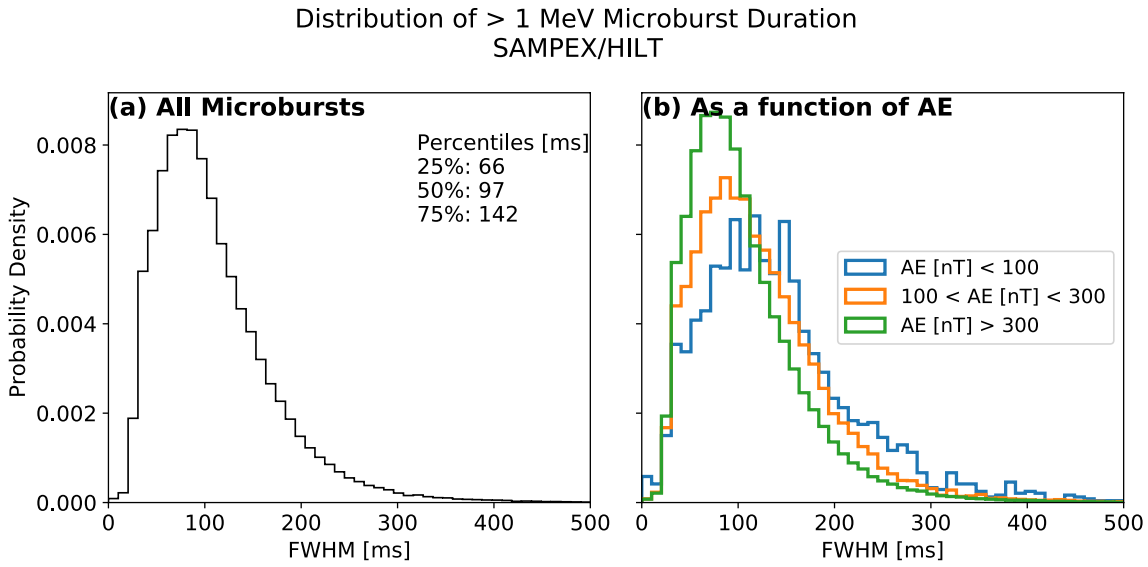

Figure 2. Panel (a) shows the distribution of all microburst full width at full maximum. Panel (b) shows the distribution of all microbursts, categorized by the Auroral Electrojet (AE) index into three bins: AE < 100, 100 < AE < 300, and AE > 300, in units of nT. The median microburst duration is 130 ms for the AE < 100 (2.4×10^3 microbursts), 111 ms for the 100 < AE < 300 (1.8×10^4 microbursts), and 95 ms for the AE > 300 (9.3×10^4 microbursts) bins.

white line, increases from 85 ms at $L = 4$, to 106 ms at $L = 5.5$. This trend is in stark contrast to Figure 4b that clearly shows the microburst duration roughly double from 75 ms near midnight to 140 ms near noon MLT.

5. Discussion and Conclusions

We found that > 1 MeV microbursts have a duration distribution peaked at ≈100 ms, with 50% of microburst durations between 66 – 142 ms. Microburst durations slightly decrease with increasing AE index. We found a significant trend in MLT—the median microburst duration doubles from 75 to 140 ms between midnight and noon MLT. However, before we put these results in the bigger context, we first need to understand how our choice of microburst detection algorithm can lead to reduced sensitivity to microbursts that are longer than ≈200 ms.

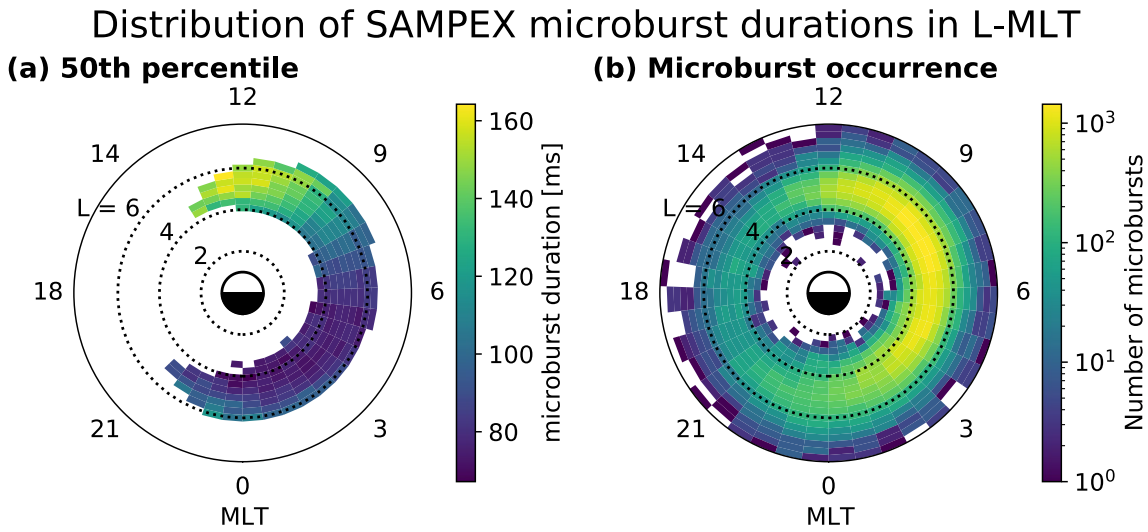

Figure 3. Panel (a) shows the joint distribution of the median microburst duration (FWHM) as a function of L-Shell and MLT. The white bins in panel a have less than 100 microbursts and are statistically insufficient. Panel (b) shows the distribution of the number of microbursts, with the white bins containing 0 microbursts.

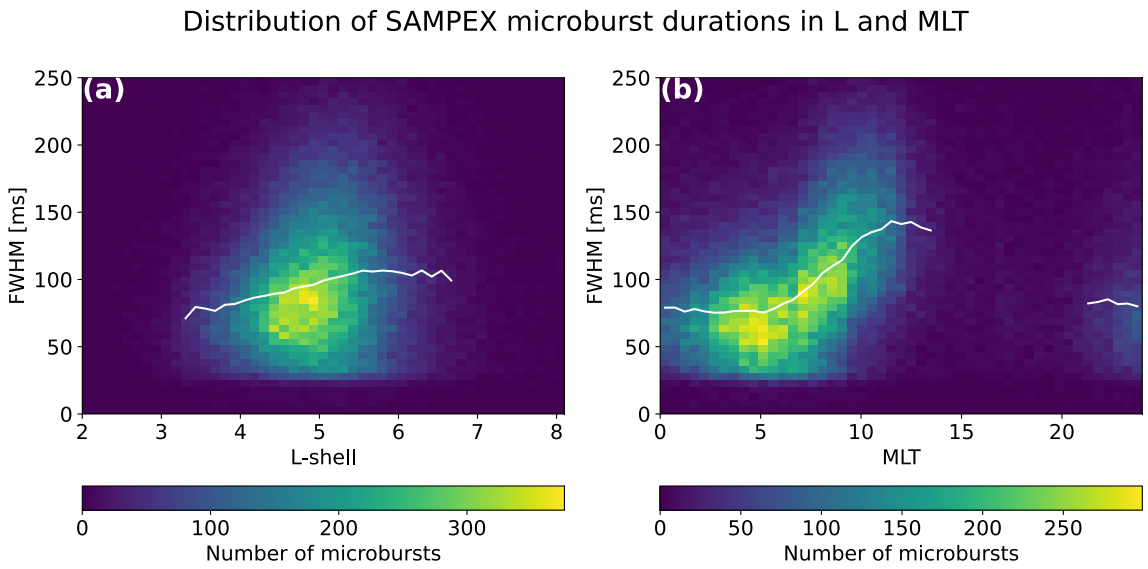

Figure 4. The marginalized distributions of the number of microbursts as a function of microburst duration (FWHM) and L-shell in panel (a), and MLT in panel (b). The white lines show the median duration in each L-shell and MLT bins.

Recall from Section 3.1 that A is the running average counts, centered on the foreground counts N, and the burst parameter, $n_\sigma \sim N - A$. Now consider the following hypothesized scenario. Given a microburst with a 500 ms duration and the burst parameter centered on the peak, A_{500} completely overlaps with the microburst and is therefore the mean microburst counts. Then, n_σ is proportional to the difference between the mean and the maximum microburst amplitude. However, if we use A_{1000}, it no longer overlaps with just the microburst, but rather the microburst and the lower surrounding background. The resulting A_{1000} is lower than A_{500}—thus the A_{1000} burst parameter is more sensitive to the microburst.

To test this possible bias, we ran the detection algorithm with three background values: A_{500}, A_{1000}, and A_{2000} and compared the resulting median distributions. The maximum discrepancy in the median microburst duration, using the three resulting data sets, was 20 ms—one HILT time sample. This is a 20% relative discrepancy. Consequently, considering this bias and the distribution in Figure 2a, the evidence supports that the majority of >1 MeV microbursts have a true duration around 100 ms and the A_{500} is adequate to identify them. With more confidence in the detection algorithm, we now discuss the global distribution of microburst durations.

The microburst duration trend in L-shell is subtle. Figure 4a shows that the median microburst duration increases from 85 to 106 ms between $L = 4$ and $L = 5.5$ and then decreases to 90 ms at $L = 7$. In contrast, the duration trend in MLT is significant. Figure 4b shows that the median microburst duration doubles from 75 to 140 ms between midnight and noon MLT. Now we will focus on the MLT trend and look for a possible explanation.

As mention in the introduction, chorus rising tone elements are widely believed to scatter microburst electrons (e.g., Breneman et al., 2017; Miyoshi et al., 2020; Saito et al., 2012). Thus, we will compare the microburst duration and chorus trends in local time. Recent studies by Teng et al. (2017) and Shue et al. (2019) quantified the properties of equatorial lower band (0.1-0.5 x electron gyrofrequency) chorus rising tone elements. Both studies found that the rising tone element duration distribution peaks at ≈250 ms around midnight, and broadening and shifting to ≈500 ms at noon. These chorus duration results and our microburst duration results both found that their durations roughly double from midnight to noon MLT. However, the chorus durations are about 3-4x longer than the microbursts. This scaling is consistent with Miyoshi et al. (2020) who predicted a similar difference in duration between chorus rising tone element and relativistic microburst durations.

As a function of AE, the median microburst duration decreases from 130 ms, for $AE < 100$ nT, to 95 ms for $AE > 300$ nT. The chorus rising tone duration trend, quantified by Teng et al. (2017), is similar: it is broad

and peaks at ≈500 ms for $AE < 100$ nT, then narrows and shifts to ≈250 ms for $AE > 300$ nT. While both become shorter with increased AE, the change in microburst duration is relatively smaller than the change in chorus duration.

Numerous test particle simulations have been performed to study the relationship between chorus rising tone elements and microbursts. Chen et al. (2020) found that medium energy (≈50 – 300 keV) microburst duration is controlled by the rising tone element bandwidth. Moreover, higher energy microburst duration is controlled by the wave's lower frequency and the absolute value of the upper magnetic latitude of propagation. Their results are in qualitative agreement with the cyclotron resonance condition described in Lorentzen et al. (2001), and the simulated electron time-of-flight described by Saito et al. (2012).

While different model parameters may change what wave properties are theoretically responsible for scattering >1 MeV microburst electrons, it is worth noting that Figures 4 and 5 in Shue et al. (2019) do not show a clear shift in chorus bandwidth between midnight and noon MLT. Care must be taken when comparing our results to theory: HILT measured multi-energy microburst electrons above 1 MeV, and microbursts at each energy can have different drivers and durations, as simulated by Chen et al. (2020) and Miyoshi et al. (2020). Nevertheless, theory does not conclusively predict what chorus wave properties control the > 1 MeV microburst duration, but the chorus rising tone duration trend in MLT is worth further consideration.

Lastly, high latitude chorus waves, observed at $|\lambda| \approx 10° - 25°$ magnetic latitudes, can also play at important role at scattering microburst electrons (Lorentzen et al., 2001). Figure 9 in Agapitov et al. (2018) shows the chorus occurrence and root-mean-square wave amplitude as a function of λ and wave normal angle in three MLT bins. In two of their MLT bins that are relevant here: 21–3 and 4–12 h, the occurrence probability is largely independent of $|\lambda|$. But this is not the case for the chorus wave amplitude; it is mostly confined to $|\lambda| < 7°$ in 21–3 MLT and $|\lambda| > 5°$ in 4–12 MLT. The chorus amplitude-MLT-$|\lambda|$ distribution, together with the time-of-flight effect, is another persuasive mechanism for differing microburst durations that is also worth further consideration.

In summary, we found that the relativistic microburst duration distribution is peaked at 100 ms, with 75% of microbursts narrower than 140 ms. We discovered a strong trend in microburst duration as a function of MLT—the median microburst duration roughly doubling from 75 ms near midnight, to 140 ms near noon. Prior work also shows that chorus rising tone element durations double in MLT (Shue et al., 2019; Teng et al., 2017). At a given local time, the rising tone element duration is 3–4 times longer. These results indicate a likely relationship between durations of chorus rising tone elements and microbursts, and we encourage future modeling work to explore this relationship.

Data Availability Statement

The SAMPEX HILT and attitude data are only available at the following FTP link http://www.srl.caltech.edu/sampex/DataCenter/data.html, and the minute cadence Auroral Electrojet data is available at ftp://ftp.ngdc.noaa.gov/STP/GEOMAGNETIC_DATA/INDICES/AURORAL_ELECTROJET/ONE_MINUTE/. This analysis software is available at: https://github.com/mshumko/sampex_microburst_widths, and is archived on Zenodo https://doi.org/10.5281/zenodo.5165064.

Acknowledgments
The authors are thankful for the engineers and scientists who made the SAMPEX mission possible. M. Shumko acknowledges the support provided by the NASA Postdoctoral Program at the NASA's Goddard Space Flight Center, administered by Universities Space Research Association under contract with NASA; L.W. Blum acknowledges the Heliophysics Innovation Fund program at NASA's Goddard Space Flight Center; and A.B. Crew acknowledges funding provided by the National Science Foundation, award 1602607.

References

Agapitov, O., Mourenas, D., Artemyev, A., Mozer, F., Hospodarsky, G., Bonnell, J., & Krasnoselskikh, V. (2018). Synthetic empirical chorus wave model from combined Van Allen probes and cluster statistics. *Journal of Geophysical Research: Space Physics*, *123*, 297–314. https://doi.org/10.1002/2017ja024843

Anderson, K. A., & Milton, D. W. (1964). Balloon observations of X rays in the auroral zone: 3. High time resolution studies. *Journal of Geophysical Research*, *69*(21), 4457–4479. https://doi.org/10.1029/JZ069i021p04457

Baker, D. N., Mason, G. M., Figueroa, O., Colon, G., Watzin, J. G., & Aleman, R. M. (1993). An overview of the solar anomalous and magnetospheric particle explorer (SAMPEX) mission. *IEEE Transactions on Geoscience and Remote Sensing*, *31*(3), 531–541. https://doi.org/10.1109/36.225519

Blake, J. B., Looper, M. D., Baker, D. N., Nakamura, R., Klecker, B., & Hovestadt, D. (1996). New high temporal and spatial resolution measurements by sampex of the precipitation of relativistic electrons. *Advances in Space Research*, *18*(8), 171–186. https://doi.org/10.1016/0273-1177(95)00969-8

Blum, L., Li, X., & Denton, M. (2015). Rapid MeV electron precipitation as observed by SAMPEX/HILT during high-speed stream-driven storms. *Journal of Geophysical Research: Space Physics*, *120*, 3783–3794. https://doi.org/10.1002/2014JA020633

Breneman, A., Crew, A., Sample, J., Klumpar, D., Johnson, A., Agapitov, O., et al. (2017). Observations directly linking relativistic electron microbursts to whistler mode chorus: Van Allen probes and FIREBIRD II. *Geophysical Research Letters*, 11265–11272. 10.1002/2017GL075001

Chen, L., Breneman, A. W., Xia, Z., & Zhang, X.-J. (2020). Modeling of bouncing electron microbursts induced by ducted chorus waves. *Geophysical Research Letters*, *47*, e2020GL089400. https://doi.org/10.1029/2020GL089400

Crew, A. B., Spence, H. E., Blake, J. B., Klumpar, D. M., Larsen, B. A., O'Brien, T. P., et al. (2016). First multipoint in situ observations of electron microbursts: Initial results from the NSF FIREBIRD II mission. *Journal of Geophysical Research: Space Physics*, *121*, 5272–5283. https://doi.org/10.1002/2016JA022485

Datta, S., Skoug, R., McCarthy, M., & Parks, G. (1997). Modeling of microburst electron precipitation using pitch angle diffusion theory. *Journal of Geophysical Research*, *102*, 17325–17333. https://doi.org/10.1029/97ja00942

Douma, E., Rodger, C., Blum, L., O'Brien, T., Clilverd, M., & Blake, J. (2019). Characteristics of relativistic microburst intensity from sampex observations. *Journal of Geophysical Research: Space Physics*, 5627–5640. https://doi.org/10.1029/2019ja026757

Douma, E., Rodger, C. J., Blum, L. W., & Clilverd, M. A. (2017). Occurrence characteristics of relativistic electron microbursts from SAMPEX observations. *Journal of Geophysical Research: Space Physics*, *122*, 8096–8107. https://doi.org/10.1002/2017JA024067

Duderstadt, K. A., Huang, C.-L., Spence, H. E., Smith, S., Blake, J. B., Crew, A. B., et al. (2021). Estimating the impacts of radiation belt electrons on atmospheric chemistry using firebird II and Van Allen probes observations. *Journal of Geophysical Research: Atmospheres*, *126*, e2020JD033098. https://doi.org/10.1029/2020JD033098

Horne, R. B., & Thorne, R. M. (2003). Relativistic electron acceleration and precipitation during resonant interactions with whistler-mode chorus. *Geophysical Research Letters*, *30*(10). https://doi.org/10.1029/2003GL016973

Johnson, A., Shumko, M., Griffith, B., Klumpar, D., Sample, J., Springer, L., et al. (2020). The FIREBIRD-II CubeSat mission: Focused investigations of relativistic electron burst intensity, range, and dynamics. *Review of Scientific Instruments*, *91*(3), 034503. https://doi.org/10.1063/1.5137905

Klecker, B., Hovestadt, D., Scholer, M., Arbinger, H., Ertl, M., Kastele, H., et al. (1993). HILT: A heavy ion large area proportional counter telescope for solar and anomalous cosmic rays. *IEEE Transactions on Geoscience and Remote Sensing*, *31*(3), 542–548. https://doi.org/10.1109/36.225520

Kurita, S., Miyoshi, Y., Blake, J. B., Reeves, G. D., & Kletzing, C. A. (2016). Relativistic electron microbursts and variations in trapped mev electron fluxes during the 8–9 October 2012 storm: Sampex and van allen probes observations. *Geophysical Research Letters*, *43*, 3017–3025. https://doi.org/10.1002/2016gl068260

Li, W., Thorne, R., Angelopoulos, V., Bonnell, J., McFadden, J., Carlson, C., et al. (2009). Evaluation of whistler-mode chorus intensification on the nightside during an injection event observed on the THEMIS spacecraft. *Journal of Geophysical Research*, *114*(A1). https://doi.org/10.1029/2008ja013554

Lorentzen, K. R., Blake, J. B., Inan, U. S., & Bortnik, J. (2001). Observations of relativistic electron microbursts in association with VLF chorus. *Journal of Geophysical Research*, *106*(A4), 6017–6027. https://doi.org/10.1029/2000JA003018

Meredith, N. P., Horne, R. B., Shen, X.-C., Li, W., & Bortnik, J. (2020). Global model of whistler mode chorus in the near-equatorial region ($|\lambda_m| < 18°$). *Geophysical Research Letters*, *47*(11), e2020GL087311. https://doi.org/10.1029/2020gl087311

Miyoshi, Y., Saito, S., Kurita, S., Asamura, K., Hosokawa, K., Sakanoi, T., et al. (2020). *Relativistic electron microbursts as high energy tail of pulsating aurora electrons*.

O'Brien, T. P., Looper, M. D., & Blake, J. B. (2004). Quantification of relativistic electron microburst losses during the GEM storms. *Geophysical Research Letters*, *31*. https://doi.org/10.129/2003GL018621

O'Brien, T. P., Lorentzen, K. R., Mann, I. R., Meredith, N. P., Blake, J. B., Fennell, J. F., et al. (2003). Energization of relativistic electrons in the presence of ULF power and MeV microbursts: Evidence for dual ULF and VLF acceleration. *Journal of Geophysical Research*, *108*. https://doi.org/10.1029/2002JA009784

Ripoll, J.-F., Claudepierre, S., Ukhorskiy, A., Colpitts, C., Li, X., Fennell, J., & Crabtree, C. (2020). Particle dynamics in the Earth's radiation belts: Review of current research and open questions. *Journal of Geophysical Research: Space Physics*, *125*, e2019JA026735. https://doi.org/10.1029/2019ja026735

Saito, S., Miyoshi, Y., & Seki, K. (2012). Relativistic electron microbursts associated with whistler chorus rising tone elements: Gemsis-rbw simulations. *Journal of Geophysical Research*, *117*, A10206. https://doi.org/10.1029/2012JA018020

Seppälä, A., Douma, E., Rodger, C., Verronen, P., Clilverd, M. A., & Bortnik, J. (2018). Relativistic electron microburst events: Modeling the atmospheric impact. *Geophysical Research Letters*, *45*, 1141–1147. https://doi.org/10.1002/2017gl075949

Shue, J.-H., Nariyuki, Y., Katoh, Y., Saito, S., Kasahara, Y., Hsieh, Y.-K., et al. (2019). A systematic study in characteristics of lower band rising-tone chorus elements. *Journal of Geophysical Research: Space Physics*, *124*, 9003–9016. https://doi.org/10.1029/2019ja027368

Shumko, M., Johnson, A. T., O'Brien, T. P., Turner, D. L., Greeley, A. D., Sample, J. G., et al. (2020). Statistical properties of electron curtain precipitation estimated with Aerocube-6. *Journal of Geophysical Research: Space Physics*, *125*, e2020JA028462. https://doi.org/10.1029/2020JA028462

Shumko, M., Turner, D. L., O'Brien, T. P., Claudepierre, S. G., Sample, J., Hartley, D. P., et al. (2018). Evidence of microbursts observed near the equatorial plane in the outer Van Allen radiation belt. *Geophysical Research Letters*, *45*, 8044–8053. https://doi.org/10.1029/2018gl078451

Summers, D. (2005). Quasi-linear diffusion coefficients for field-aligned electromagnetic waves with applications to the magnetosphere. *Journal of Geophysical Research*, *110*. https://doi.org/10.1029/2005JA011159

Teng, S., Tao, X., Xie, Y., Zonca, F., Chen, L., Fang, W., & Wang, S. (2017). Analysis of the duration of rising tone chorus elements. *Geophysical Research Letters*, *44*, 12074–12082. https://doi.org/10.1002/2017gl075824

Thébault, E., Finlay, C. C., Beggan, C. D., Alken, P., Aubert, J., Barrois, O., et al. (2015). International geomagnetic reference field: The 12th generation. *Earth Planets and Space*, *67*(1), 79. https://doi.org/10.1186/s40623-015-0313-0

Thorne, R. M. (2010). Radiation belt dynamics: The importance of wave-particle interactions. *Geophysical Research Letters*, *37*. https://doi.org/10.1029/2010GL044990

Thorne, R. M., O'Brien, T. P., Shprits, Y. Y., Summers, D., & Horne, R. B. (2005). Timescale for MeV electron microburst loss during geomagnetic storms. *Journal of Geophysical Research*, *110*(A9). https://doi.org/10.1029/2004JA010882

Winckler, J., Bhavsar, P., & Anderson, K. (1962). A study of the precipitation of energetic electrons from the geomagnetic field during magnetic storms. *Journal of Geophysical Research*, *67*(10), 3717–3736. https://doi.org/10.1029/jz067i010p03717